ELSEVIER

Physica B 244 (1998) 138–147

PHYSICA B

Spin, charge, and bonding in transition metal mono-silicides

D. van der Marel[a,*], A. Damascelli[a], K. Schulte[a], A.A. Menovsky[b]

[a] *Solid State Physics Laboratory, University of Groningen, Groningen 9747 AG, The Netherlands*
[b] *University of Amsterdam, 1018 XE Amsterdam, The Netherlands*

Abstract

We review some of the relevant physical properties of the transition metal mono-silicides with the FeSi structure (CrSi, MnSi, FeSi, CoSi, NiSi, etc.) and explore the relation between their structural characteristics and the electronic properties. We confirm the suggestion orginally made by Pauling that the FeSi structure supports two quasi-atomic d-states at the transition metal atom. This shell contains from 0 to 4 electrons in the sequence CrSi to NiSi. In FeSi the two quasi-atomic d-electrons are responsible for the high temperature $S = 1$ state, which is compensated for $T = 0$ by two itinerant electrons associated with the Fe–Si resonance bonds. Published by Elsevier Science B.V.

Keywords: FeSi; Mono-silicides

1. Introduction

Among the large variety of unusual properties found in transition metal compounds, the phenomenon of spin-singlet formation is one of the most intrigueing, and perhaps the most widely spread. The impact of singlet formation on the physical state ranges from insulating behaviour to superconductivity. In some cases singlet formation is accompanied by a spin-Peierls lattice deformation, such as in $CuGeO_3$. In other cases the formation of singlets is accompanied by a transition from a metallic to an insulating state. It has been suggested that FeSi is such a Kondo-insulator [1–3]. In the present paper we discuss the wider class of transition metal mono-silicides (CrSi, MnSi, FeSi, CoSi, NiSi, etc.) with the FeSi structure, we review the structural and physical data of this class of compounds, and explore the relation between their structural characteristics and the electronic properties.

* Corresponding author.

0921-4526/98/$19.00 Published by Elsevier Science B.V.
PII S0921-4526(97)00476-6

2. Structural properties

In Table 1 we summarize the lattice structures of the mono-silicides for the various d-transition elements (for Ru, Os and RhSi, see Ref. [4]; for ReSi see Ref. [5] and for Cr, Mn, Fe, Co and NiSi see Ref. [6]). For the 3d series the $T^4 - P2_13$ space group has been observed from CrSi to NiSi. For NiSi in addition the NiAs structure has been reported. The $T^4 - P2_13$ space group has also been reported for RuSi, RhSi, ReSi and OsSi. TiSi, VSi, PdSi, IrSi and PtSi all have the MnP structure.

In this paper we restrict the discussion to the mono-silicides with the $T^4 - P2_13$ space

Table 1
Lattice parameter (a), displacement vectors x (units of lattice constant a), interatomic distances between TM and Si atoms (d_1, d_2, d_3), weighted average of the latter (d) and the sum of the atomic radii for 12-coordinated metals and the single bond radius of Si (d_{sum}). For CoSi and NiSi no published values of x could be located

	a (Å)	x_{TM} (a)	$1 - x_{Si}$ (a)	d_1 (Å)	d_2 (Å)	d_3 (Å)	d (Å)	d_{sum} (Å)
ReSi	4.775	0.14	0.16	2.5	2.5	2.7	2.56	2.55
OsSi	4.728	0.128	0.161	2.364	2.429	2.715	2.54	2.52
RuSi	4.701	0.128	0.164	2.383	2.395	2.706	2.53	2.51
RhSi	4.676	0.147	0.155	2.451	2.480	2.548	2.51	2.52
CrSi	4.629	0.136	0.154	2.325	2.435	2.589	2.49	2.45
MnSi	4.558	0.138	0.154	2.305	2.402	2.537	2.45	2.43
FeSi	4.493	0.136	0.156	2.271	2.352	2.519	2.41	2.44
CoSi	4.447	0.14?	0.16?	2.2?	2.3?	2.5?	2.4?	2.42
NiSi	4.437	0.14?	0.16?	2.2?	2.3?	2.5?	2.4?	2.42

group (displayed in Fig. 1). This simple cubic structure contains four TM atoms in the positions $(x, x, x; x + \frac{1}{2}, \frac{1}{2} - x, 1 - x$; et cycl.) and four Si atoms in an equivalent set.

In Table 1 we summarize the cell-parameters and the interatomic distances [4–6]. The four transition metal and silicon atoms occupy equivalent sites. The site symmetry has only a three-fold rotation axis, which we indicate throughout this paper as the local z-axis. The TM-atom has a 7-fold coordination by Si atoms and vice versa: A single bond pointing toward the Si-atom along the z-axis (type 1), and two groups of three indentical bonds (types 2 and 3) with azimuthal angles relative to the z-axis of 0° (type 1) 74° (type 2) and 141° (type 3). The two groups of types 2 and 3 are rotated around the local z-axis with an angle of 24° ± 2° relative to each other. The four equivalent sites within the unit cell have the same sense of rotation, hence two isomeric structures (left-handed and right-handed) exist. As a result phase/anti-phase boundaries of the two isomers can occur (also in single crystals) which may will considerable influence on the transport properties. Single domain crystals should exhibit optical activity. These aspects of the transition metal monosilicides still await further scrutiny.

Within an accuracy of 2% the average distance between the TM-atom and its 7 Si neighbours (d) follows the rule $d = r_{TM} + r_{Si}$, where r_{TM} is the atomic radius of the TM atom in 12-coordinated metals [7], and $r_{Si} = 1.173$ Å is the single bond radius of Si (Fig. 2 and Table 1), indicating that almost no charge transfer takes place between Si and the TM atom. The absence of charge transfer between TM and Si can be anticipated from the fact that the Pauling electronegativities are almost the same.

For $x(TM) = 0.1545$ and $x(Si) = -0.1545$ all seven neighbours have the same bondlength. As we can see in Table 1 the structure of the TM-monosilicides is rather close to this situation, but the deviations are significant. The variation of the bondlength within the group of 7 nearest neighbours has been discussed by Pauling [8] for CrSi to NiSi in terms of valence bond sums, which lead to the following bond numbers: one full bond (type 1), three $\frac{2}{3}$ bonds(type 2) and three $\frac{1}{3}$ bonds (type 3).

3. Electronic properties

3.1. Magnetic properties

The best studied materials in this class are MnSi and FeSi. MnSi has a helical spin structure at low fields below the Neèl temperature of 29 K, and is paramagnetic above T_N. CrSi and

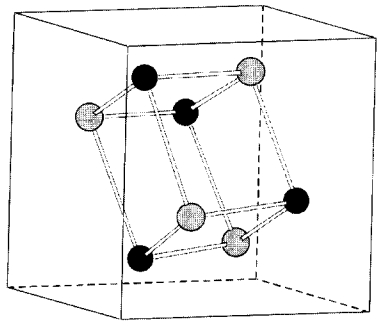

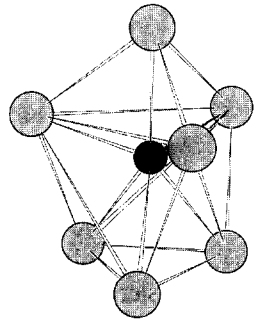

Fig. 1. Crystal structure with the $T^4 - P2_13$ space group, and a $TMSi_7$ cluster representing the site symmetry of individual atoms in this structure.

NiSi are either weakly paramagnetic or diamagnetic. Estimates of the local moment on Mn based on magnetic susceptibilities vary from $\mu_{eff} = 2.12\mu_B$ with $g = 2$ below 300 K to $3.3\mu_B$ above 600 K [9–11]. For FeSi [12] the high temperature limiting behaviour of the susceptibility gives $\mu_{eff} = 1.7$ with $g = 3.9$, but good fits to thermally activated Curie–Weiss behaviour were also obtained with $\mu_{eff} = 2.8$ and $g = 2$.

3.2. Optical properties

In Fig. 3 we reproduce the real part of the optical conductivity and of dielectric constants for some selected temperatures of FeSi and CoSi. In Fig. 4

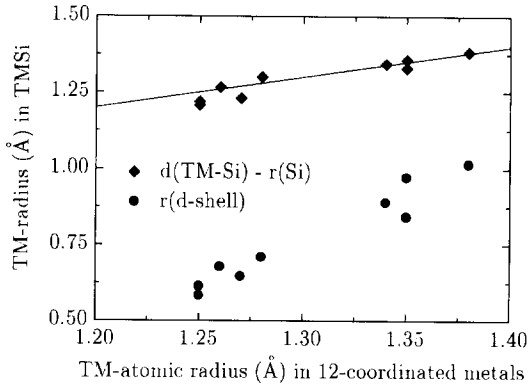

Fig. 2. TM radius in TM-Si (TM-Si bondlength minus radius of Si, diamonds) and d-shell radii (circles) versus the TM radius in 12-coordinated metals.

we display the function $Nm_e/m^*(\omega) = 2m_e\pi^{-1}q_e^{-2}n_{TMSi}^{-1}\int_0^\omega \sigma(\omega)\,d\omega$ for both compounds. The high frequency limit corresponds to the total number of electrons per FeSi (i.e. 40 electrons). Here we neglected the contribution of the nuclei, which is justified due to the large ratio of the nuclear mass compared to the electron mass. We see, that for CoSi the $Nm_e/m^*(\omega)$-curves for different temperatures merge above 1000 cm^{-1} indicating that no transfer of spectral weight from high to low frequencies takes place.

For FeSi the recovery of spectral weight can be followed upto approximately 2000 cm^{-1} above which the experimental errorbars become rather large as a result of uncertainties in the Kramers–Kronig analysis, mainly induced by the extrapolations at high frequency [13, 14]. It seems plausible to associate the temperature dependence of the section between 1000 and 2000 cm^{-1} with the optical conductivity due to thermally induced charge carriers. In Fig. 5 this number is displayed versus temperature along with the Hall number of Chernikov et al. [15]. We display $Nm_e/m^*(\omega)$ for 3 different values of the cutoff frequency (ω = 300, 800 and 2000 cm^{-1}) to demonstrate that the activation energy is independent of frequency. We observe that the Hall number and Nm_e/m^* have approximately the same activation energy of about 200–250 K.

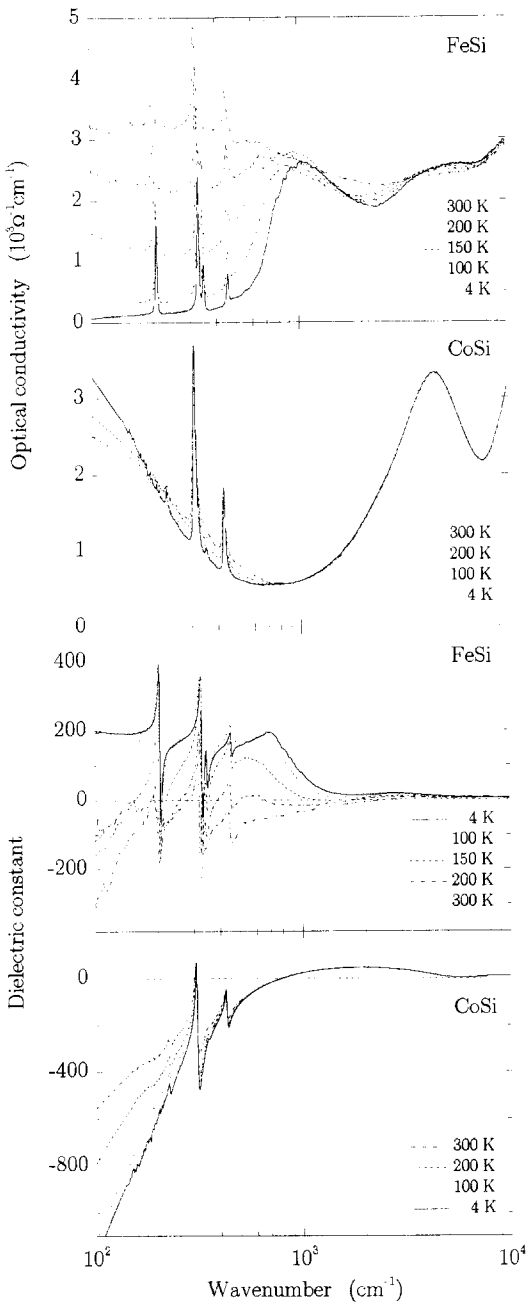

Fig. 3. Real part of the optical conductivity (σ_1) and of the dielectric constant (ε') of FeSi and CoSi.

3.3. Activation energies

In Table 2 we collect the activation energies and gap values determined from various spectroscopic

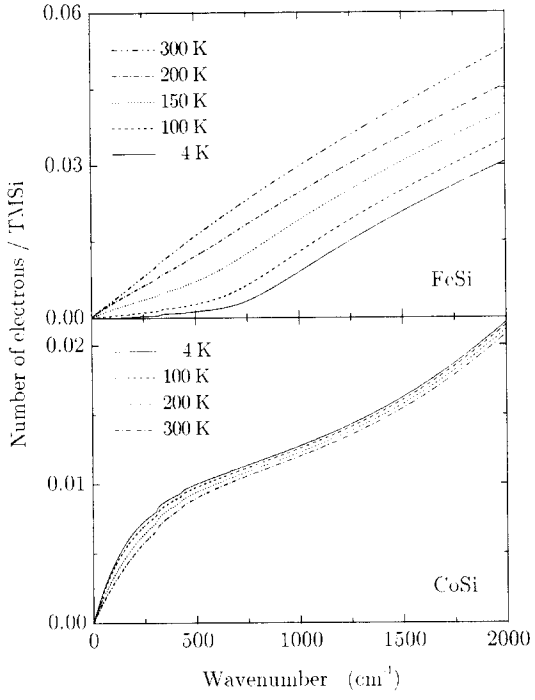

Fig. 4. Number of carriers per TMSi versus frequency (ω) obtained from partial integration of the optical conductivity upto ω.

data and transport properties. For the tunneling data the gap-value corresponds to the peak-to-peak-value in the dI/dV versus V curves. In a single particle band picture this value should match the optical and Raman gap. Clearly there is a rather large spread of activation energies. The trend is, that the higher the temperature range considered, the larger the activation energy obtained. This indicates, that the thermal evolution involves a distribution of activation energies.

3.4. Transport properties

The behaviour of the electrical resistivity of FeSi and CoSi is quite different (see Fig. 6). CoSi has a high residual resitance and conventional Bloch–Grüneisen behaviour. FeSi shows insulating behaviour at low temperature. The DC resistivity of FeSi $\rho = m^*/(ne^2\tau)$ varies from 2500

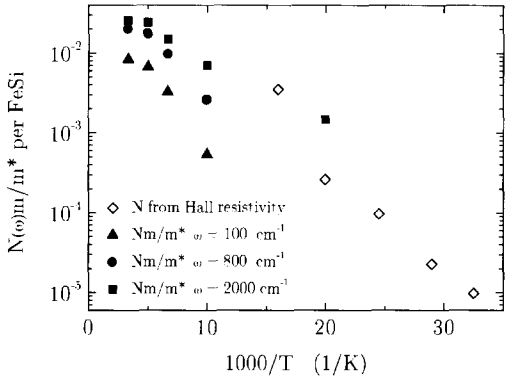

Fig. 5. Number of carriers per unit of FeSi from integrating the optical conductivity (closed symbols) and Hall conductivity (open diamonds).

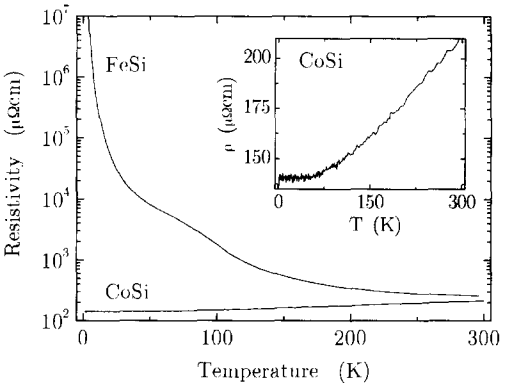

Fig. 6. Resistivity of FeSi and CoSi.

Table 2
Compilation of activation energies observed for FeSi. For tunneling, Raman spectroscopy and infrared spectroscopy the indicated value corresponds to the gap divided by two. K(Si) is the activation energy of the Knight shift at the Si nucleus, Q(Fe) of the nuclear quadrupole splitting of Fe observed with Mössbauer spectroscopy

Exp. method	Source	Temp. (K)	E_a (meV)
Tunneling	Ref. [16]	4	43
IR spectr.	Ref. [17]	4	38
Raman	Ref. [18]	4	47
K(Si)	Ref. [19]	< 800	41
$\chi(T)$	Ref. [12]	< 800	68
Q(Fe)	Ref. [19]	< 800	46
n(Hall)	Ref. [15]	< 100	22
n(IR)	This work	> 100	22
ρDC	This work	> 100	30

to 300 μΩ cm between 100 and 300 K. When combined with the carrier densities of Fig. 5 we see that τ varies from 4.6 to 10 fs between 100 and 300 K. Note that the same ratio n/m^* appears in the Drude expression as in the expression of the optical carrier density. Hence our result for τ does not depend on assumptions for the effective mass. An estimate of the carrier life-time τ is also obtained from direct inspection of $\sigma(\omega,T)$. As there are no thermally excitated carriers at 4K we proceed by subtracting $\sigma(\omega,4\text{ K})$ from the conductivity spectra at higher temperature. In the zeroth approximation the increase in conductivity upon raising temperature is a Drude–Lorentzian due to the thermally excited carriers. At the gap frequency and the optical phonons the difference spectra contain quirks due to the shifting of the gap, and thermal broadening of the phonons. Otherwise the difference curves have a halfwidth of $500 < (2\pi c\tau)^{-1} < 1000\text{ cm}^{-1}$, or 10 fs > τ > 5 fs, in good agreement with the life-time calculated from the DC resistivity.

Let us first explore the possibility that the excited carriers can be described in the same way as in conventional doped semiconductors. The carrier density and k_F are related through $n_e = gk_F^3/(6\pi^2)$, where g is the overall degeneracy factor (valley and spin). Band theory predicts a 12-fold degeneracy of the electron pockets, and an 8-fold degeneracy of the hole pockets [20, 21]. To simplify matters we will ignore possible differences in mass and mobility for electrons and holes. Hence the degeneracy factor entering the optical carrier density is $g = 2\times(8 + 12) = 40$. The observed density n_e varies from 0.3 to $1.3\times10^{21}\text{ cm}^{-3}$ (100–300 K), implying that k_F varies from 4.9 to $7.5\times10^6\text{ cm}^{-1}$, v_F varies from 5.6 to 8.7×10^4 m/s and E_F varies from 9 to 21 meV. Hence the electrons and holes are essentially nondegenerate throughout this temperature range as expected for thermal excitation across a semiconductor gap. Using our estimate of v_F we calculate a mean free path of 2.6–9.0 Å for temperatures in the range of 100–300 K. This mean

free path is sufficiently short to smear the momentum of the charge carriers on the scale of the size of the electron and hole pockets ($0.02 < k_F l/(2\pi) < 0.1$), and even sufficient to smear the momentum over the entire Brillouin zone ($0.5 < l/a < 2$). This implies that the conduction of the charge carriers is essentially of the hopping type. However, this small value of l implies that the fine details of the bandstructure become irrelevant, and the multi-valleyed character of electron and hole pockets is scrambled, thus invalidating the assumption made on the input that $g = 40$.

Let us now compare the absolute values of the carrier density in Fig. 5 obtained from the Hall effect and from optical conductivity. If we extrapolate the Hall number to the region between 100 and 300 K where we have reliable estimates of the optical carrier density (Nm_e/m^*), the Hall number seems to overshoot Nm_e/m^* with a factor of 5–10. In a semiconductor model with equal electron and hole masses and mobilities the optical carrier density corresponds to $n_{opt} = n_e + n_h$, whereas $1/n_{Hall} = 1/n_e - 1/n_h$. There is a compensation between electron and hole contributions to the Hall constant, leading to an experimental Hall number which is always larger than the optical carrier density.

The combination of electron-like Hall conductivity, and short mean free path of the carriers, motivates us to propose a different scenario from the semiconductor picture which we explored above: The effect of raising temperature is to excite electrons to a wide band above the Fermi energy. The holes which are left behind move within a narrow band of (almost) localized states. From the perspective of the effect on doping the latter states behave in the same way as donor states in a conventional semiconductor, but should be really understood as a narrow band of quasi-atomic states of the transition metal atoms. As we may now ignore the contribution to the charge response of the hole channel (due to the low mobility) the smaller value of the optical carrier density Nm_e/m^* compared to the (extrapolated) Hall number in the 100–300 K range indicates a moderate effective mass of the mobile charge carriers $m^*/m_e \approx 5$–10. An explicit realization of this situation is the pairing of itinerant electrons with local moments at low temperature to form a lattice of Kondo-singlets [13]. At sufficiently high temperatures these singlets will be broken into their constituents, i.e. itinerant electrons and local moments. As no mobile charges are associated with the local moments, these moments add a neglegible contribution both to the Hall conductivity and the infrared conductivity, so that the dominant contribution comes from the thermally excitated itinerant electrons. A natural consequence of having unpaired local moments at higher temperatures is spin-flip scattering of the itinerant electrons, leading to a reduction of the mean free path. This scattering mechanism will be suppressed if the local moments are aligned by the external application of a magnetic field (positive magneto-conductivity).

Motivated by these arguments we recalculate the carrier properties, adopting a degeneracy factor $g = 2$ (only spin): k_F now varies from 1.3 to $2.0 \times 10^7\ \mathrm{cm}^{-1}$, v_F varies from 1.5 to 2.4×10^5 m/s, E_F from 66 to 160 meV, l from 7.0 to 25.0 Å, and $k_F l/2\pi$ from 0.15 to 0.8.

3.5. Resonating bonds coupled to phonons

The steps in the $Nm_e/m^*(\omega)$ curve in Fig. 4 at frequencies below $1000\ \mathrm{cm}^{-1}$ are due to optical phonons [22]. By applying the optical sum-rule to these vibrational resonances we can determine the dynamical (or transverse effective) charge of Fe and Si for each temperature. For a purely ionic insulator this is also the actual charge of the ions. For a covalent compound with resonating bonds a finite value of the transverse effective charge results from a dynamical charge redistribution associated with the ionic motion of an optical phonon. For the TM mono-silicides Pauling has argued that resonance occurs between the partial bonds of types 2 and 3 ($\frac{1}{3}$ and $\frac{2}{3}$ bonds). Lucovsky and White [23] have shown (for the IV–VI narrow gap semiconductors) that this phenomenon leads to a high value of the transverse effective charge. Rice, et al. [24] developed the theory for the infrared spectra for phonons coupled to charge excitations.

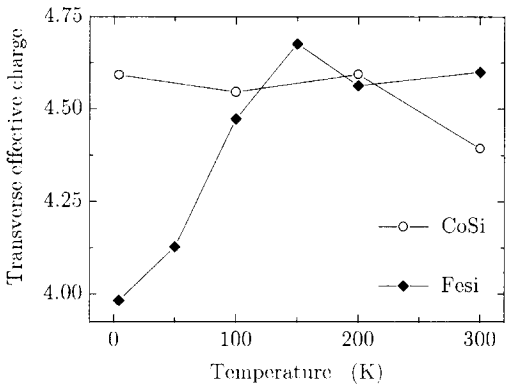

Fig. 7. Transverse effective charge of Fe–Si and Co–Si pairs calculated from the oscillator strength of the optical phonons.

In Fig. 7 we display the transverse effective charge for both compounds. A large value of more than 4 is found for Z^{eff}. Based on the electronegativities and from the observed atomic radii there can be almost no charge transfer between the transition metal atom and Si in these compounds. Hence we attributed the large value of the transverse effective charge to a dynamical coupling of the optical phonons to electronic resonances. The full analysis was presented in Ref. [17]. This requires that at least some of the bonds between Fe and Si are incomplete. The enhancement of transverse effective charge is then due to a coupling of the ionic displacement to charge flow between the unsaturated bonds.

4. The electronic structure of TMSi

From ab initio bandstructure calculations for FeSi it is known, that in these materials the Si-3s states are fully occupied and have a binding energy of about 10 eV. The Si 3p states are partially occupied and form together with the TM-states a complex manifold of bands.

According to a famous rule from the theory of Mott–Hubbard metal-insulator transitions the atomic description of the TM atom becomes the appropriate ansatz if the on-site correlation energy exceeds the bandwidth. For the TM silicides the bandwidth is of order 6 eV, and U^{eff} is of the same order of magnitude. The silicides therefore seem to provide a border case. A band description where the correlation effects are taken into account perturbatively has been used by several investigators [21, 25–27]. In this paper we want to explore a more intuitive approach based on an atomistic picture.

In their elemental metallic phase the TM atoms have approximately a $d^{n-2}s^2$ configuration, with n the number of valence electrons per atom. From the d-shell radii displayed in Fig. 2 we can see, that in the whole series the d-shell radius [28] falls well below the atomic radius, which implies that the d-shells exhibit quasi atomic characteristics due to shielding by the outer s and p-shells. Due to the low site symmetry of the TM-atoms mixing of s, p and d-character occurs in the eigenstates. For the purpose of compactness of notation we will label the TM valence bands as 'd'-states. We will assume that these states have quasi-atomic characteristics, so that we can use a ligand field description to describe the influence of the Si-matrix. For the purpose of bookkeeping of the actual d- and sp-count of the atoms, it is important to take into account the relative contribution of s and p character to the 'd'-states.

With this approach we arrive at the following scenario: Each TM atom contributes five d-states and n electrons. In the case of FeSi: $n = 8$. Each Si contributes three 3p states and four electrons. Due to the 3-fold rotation symmetry the five d-states are grouped in a single degenerate $d_0(z^2)$ state, and two groups of doubly degenerate levels (E^+ and E^-) corresponding to linear combinations of d_{-2}, d_{-1}, d_1 and d_2. Here we adopted a local reference frame with the z-axis oriented along the 3-fold rotation axis which pierces the TM atom. Of the surrounding shell of seven Si atoms only the 3p orbitals with their lobes pointing toward the transition metal atom couple to the TM states. Thus seven ligand orbitals are engaged in bonds with the TM-atom. We indicate the ligand of type 1 as $|L_{0,1}\rangle$. Taking into account the hopping τ between the Si atoms at relative angles $\phi = 0$, $\pi/3$ and $2\pi/3$, we obtain the ligand-states of all types $j (j = 1, 2, 3)$:

$$|L_{0,j}> = |p_0> + |p_{+\eta}> + |p_{-\eta}>,$$

$$E_0 = \varepsilon_p - 2\tau,$$

$$|L_{+,j}> = |p_0> + e^{2\pi i/3}|p_{+\eta}> + e^{-2\pi i/3}|p_{-\eta}>,$$

$$E_+ = \varepsilon_p + \tau,$$

$$|L_{-,j}> = |p_0> + e^{-2\pi i/3}|p_{+\eta}> + e^{2\pi i/3}|p_{-\eta}>,$$

$$E_- = \varepsilon_p + \tau.$$

The degeneracy between the ligand states $|L_{\pm,j}>$ with $j = 2$ and 3 is lifted due to a finite hopping probability between these groups:

$$\langle L_{\pm 2}|H|L_{\pm,3}\rangle = \tau'.$$

The dependence on the angular coordinate ϕ of the hopping integral between the $d_{\pm 2}$ ($d_{\pm 1}$) and the ligand 3p orbital is $e^{\pm 2i\phi}$ ($e^{\pm i\phi}$). The angle η_j identifies the orientation of the two rings of ligand Si atoms: $\eta_j = 0°$ resp. 24° for type $j = 2$ resp. 3. The resulting (nonzero) hopping matrix elements between the ligand orbitals and the central TM atom are with this choice of local reference frame:

$$\langle d_0|H|L_{0,j}\rangle = t_{0,j},$$

$$\langle d_{\pm 1}|H|L_{\pm,j}\rangle = t_{1,j}e^{\mp i\eta_j},$$

$$\langle d_{\pm 2}|H|L_{\pm,j}\rangle = t_{2,j}e^{\pm 2i\eta_j}.$$

All other matrix elements are zero. In principle, all ligand combinations of the $TMSi_7$ cluster are shared between neighbouring TM-sites and form bands. Due to the angle of $\simeq 70°$ between the bonds of types 2 and 3, we anticipate that a linear combination of $d_{\pm 1}$ and $d_{\pm 2}$ exists which has a strongly reduced hopping matrix element to the cluster of ligand orbitals, resulting in a (doubly degenerate) non-bonding orbital of a quasi-atomic character. The resulting level scheme of hybrid TM-ligand character is sketched in Fig. 8. The single (per TM atom) axial bonding orbitals of $d_0 - L(1)$ character have the highest binding energy, followed by a band containing the two states of bonding $d(E^-) - L_{\pm}(2, 3)$ character. Around E_F we find a combined partially occupied anti-bonding band, containing three states in total. Finally two non-bonding $d(E^+)$ states are located at E_F. With a finite value for the hopping parameter

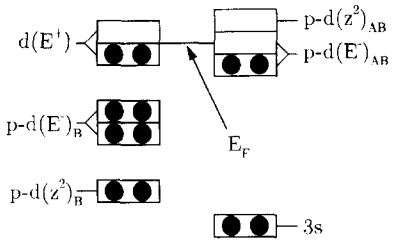

Fig. 8. Schematic diagram of the energy levels in TMSi. The situation with two electrons in the $d(E^+)$ level which is displayed here corresponds to FeSi.

of these states to the ligand orbitals taken into account, the latter states form a narrow band. Provided that the width of this band is sufficiently small, it behaves as a lattice of quasi-atomic open shells obeying Hund's rules. The observation that two quasi-atomic d-states with two electrons per Fe atom should exist in FeSi was originally made by Pauling, using a different line of argueing, based on his analyses of the valence bond sums [8].

We conjecture that these subshells are filled step by step in the series CrSi (zero electrons/atom) upto NiSi (four electrons/atom). This leaves two electrons per Si atom to populate the more itinerant anti-bonding band at E_F. This partly filled anti-bonding band corresponds to partial bonds of type 2 and 3, and is responsible for the strong enhancement of the transverse dynamical charge in CoSi and FeSi [17].

This scenario provides a qualitative argument why the same crystal structure is observed from CrSi upto NiSi: Only if electrons are added to – or removed from – the itinerant anti-bonding band, chemical bonds are affected, and the FeSi structure is de-stabilized. Addition or removal of electrons from this wide band will not take place unless the $d(E^+)$ subshell is either completely full or empty, e.g. for VSi or CuSi. It is now easy to understand the high spin state of FeSi at elevated temperatures: The electrons in the itinerant band contribute a Pauli-paramagnetic susceptibility, which is small. According to Hund's rules the two electrons in the $d(E^+)$ subshell are in a triplet configuration, thus providing the Curie-susceptibility with $S = 1$ and

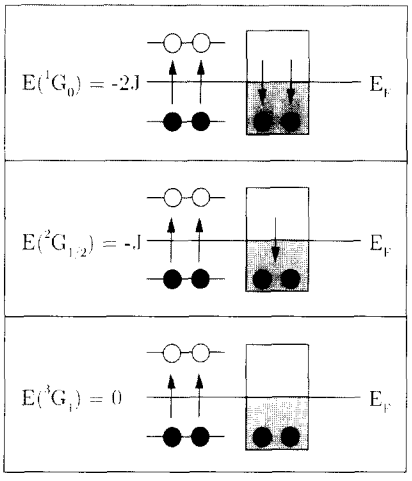

Fig. 9. Schematic diagram of the relevant low energy degrees of freedom of FeSi. The top panel corresponds to the singlet low temperature phase, the bottom panel to the high temperature $S = 1$ phase, and the middle panel represents an intermediate situation with a partial compensation of the local moment.

$g = 2$ that has been observed at high temperatures. In Fig. 9 the relevant elements for the low energy scale are sketched: One local moment with $S = 1$ at every site, exchange-coupled to a band with two conduction electrons per site.

5. Conclusions

Based on a discussion of infrared and transport data presented in this report and of published data, we provide a qualitative model of the electronic structure of the transition metal monosilicides. The main conclusion is that six electrons per transition metal atom are engaged in chemical bonds to the Si sublattice. The remaining electrons of the TM atoms (two for FeSi) occupy a doubly degenerate quasi-atomic d-state, and obey Hunds rules. The conduction band supports two weakly bound itinerant electrons (mainly Si 3p character) which in the case of FeSi compensate the local moment at low temperatures by forming a Kondo singlet. This framework provides a basis for understanding the observed range of chemical stability of these compounds (CrSi to NiSi), and of the physical properties of FeSi.

Acknowledgements

We gratefully acknowledge M. Fäth for communicating his results to us prior to publication. This investigation was supported by the Netherlands Foundation for Fundamental Research on Matter (FOM) with financial aid from the Nederlandse Organisatie voor Wetenschappelijk Onderzoek (NWO).

References

[1] G. Aeppli, in: K.S. Bedell et al. (Eds.), Strongly Correlated Electron Materials, Addison-Wesley, Reading, MA, 1994, p. 3.
[2] D. Mandrus, J.L. Sarrao, A. Migliori, J.D. Thompson, Z. Fisk, Phys. Rev. B 51 (1995) 4763.
[3] C.-H. Park, Z.-X. Shen, A.G. Loeser, D.S. Dessau, D.G. Mandrus, A. Migliori, J. Sarrao, Z. Fisk, Phys. Rev. B 52 (1995) R16981.
[4] K. Göransson, I. Engström, B. Noläng, J. Alloys Compounds 210 (1995) 107.
[5] R.A. Mc Nees, A.W. Searcy, J. Am. Chem. Soc. 77 (1955) 4290.
[6] B. Borén, Ark. Kemi Min. Geol. 11A (1933) 1.
[7] W.B. Pearson, Crystal Chemistry and Physics of Metals and Alloys, Wiley, New York, 1972.
[8] L. Pauling, A.M. Soldate, Acta Crystallorgr. 1 (1948) 212.
[9] F.A. Sidorenko et al., Sov. Phys. J. 12 (1969) 329.
[10] Z. Radovskii et al., Sov. Phys. J. 8 (1965) 98.
[11] G. Foëx, J. Phys. Radium 9 (1938) 37.
[12] V. Jaccarino, G.K. Wertheim, J.H. Wernick, L.R. Walker, S. Arajs, Phys. Rev. 160 (1967) 476.
[13] Z. Schlesinger, Z. Fisk, Hai-Tao Zhang, M.B. Maple, J.F. DiTusa, G. Aeppli, Phys. Rev. Lett. 71 (1993) 1748.
[14] L. Degiorgi, M.B. Hunt, H.R. Ott, M. Dressel, B.J. Feenstra, G. Grüner, Z. Fisk, P. Canfield, Europhys. Lett. 28 (1994) 341.
[15] M.A. Chernikov, E. Felder, S. Paschen, A.D. Bianchi, H.R. Ott, J.L. Sarrao, D. Mandrus, Z. Fisk, Physica B 230 (1997) 790.
[16] M. Fäth, J. Aarts, G.J. Nieuwenhuys, A.A. Menovsky, J.A. Mydosh, Phys. Rev. B, submitted.
[17] A. Damascelli, K. Schulte, D. van der Marel, A.A. Menovsky, Phys. Rev. B 55 (1997) R4863.
[18] P. Nyhus, S.L. Cooper, Z. Fisk, Phys. Rev. B 51 (1995) 15626.

[19] G.K. Wertheim, V. Jaccarino, J.H. Wernick, J.A. Seitchik, H.J. Williams, R.C. Sherwood, Phys. Lett. 18 (1965) 89.
[20] L.F. Mattheiss, D.R. Hamann, Phys. Rev. B 47 (1993) 13114.
[21] V.I. Anisimov, S.Y. Ezhov, I.S. Efimov, I.V. Solovyev, T.M. Rice, Phys. Rev. Lett. 76 (1996) 1735.
[22] A. Damascelli, K. Schulte, D. van der Marel, J. Mydosh, M. Faeth, J. Aarts, A.A. Menovsky, Physica B 230 (1997) 787.
[23] G. Lucovsky, R.M. White, Phys. Rev. B 8 (1973) 660.
[24] M.J. Rice, N.O. Lipari, S. Strässler, Phys. Rev. Lett. 39 (1977) 1359.
[25] Y. Takahashi, T. Moriya, J. Phys. Soc. Japan 46 (1979) 1451.
[26] S.N. Evangelou, D.M. Edwards, J. Phys. C 16 (1983) 2121.
[27] C. Fu, M.P.C.M. Krijn, S. Doniach, Phys. Rev. B 49 (1994) 2219.
[28] D. van der Marel, G.A. Sawatzky, Phys. Rev. B 37 (1988) 10674.